ChemComm

Nanozyme-like colorimetric sensing strategy based on persulfate activation on Co-based metal-organic frameworks

Journal:	*ChemComm*
Manuscript ID	CC-COM-01-2023-000249.R1
Article Type:	Communication

COMMUNICATION

Nanozyme-like colorimetric sensing strategy based on persulfate activation on Co-based metal-organic frameworks

Received 00th January 20xx,
Accepted 00th January 20xx

DOI: 10.1039/x0xx00000x

Zehui Deng,[a] Qingling Xiao,[b] Heyun Fu,[a] Shourong Zheng,[a] Pedro J.J. Alvarez,[c] Dongqiang Zhu,[d] Zhaoyi Xu*[a] and Xiaolei Qu *[a]

A nanozyme-like colorimetric sensing strategy based on persulfate activation on Co-based metal-organic frameworks is developed for biomolecule detection in solutions and on paper strips. By switching from H_2O_2 activation on nanozymes to catalytic persulfate activation, this general strategy provides higher sensitivity, faster speed, and wider application ranges for detection.

Nanozymes are a class of mimic enzymes that have both the unique properties of nanomaterials and the catalytic functions of enzymes.[1] They are widely used in colorimetric sensors due to their high catalytic activity, stability, convenience, and feasibility for large-scale production compared with natural enzymes.[2,3] Nanozyme-based colorimetry for biomolecule detection gained significant interest as it is low-cost, easy to distribute and use, and ideal for real-time clinic diagnosis.[4,5] In nanozyme-based colorimetric sensors, hydrogen peroxide (H_2O_2) is activated on peroxidase-like nanozymes to produce hydroxyl radicals (•OH), which in turn oxidize chromogenic substrates (*e.g.*, 3,3',5,5'-tetramethylbenzidine, TMB) to induce color changes. The presence of biomolecules can inhibit the color change by competing for •OH, occupying the active sites, or reducing oxidized TMB (oxTMB), which is then used for quantification.[6] Nevertheless, the applications of colorimetric sensors based on H_2O_2 activation on nanozymes are still limited by their sensitivity,[6, 7] applicable pH range,[5, 8] and detection speed.[6, 9, 10]

Recently, persulfate-based advanced oxidation processes (AOPs) have drawn broad interest in overcoming limitations of the environmental remediation field.[11] The main radical generated in persulfate-based AOP is sulfate radical ($SO_4^{\bullet-}$), which has higher redox potential (E^0 = 2.5-3.1 V) and much longer half-life (~ 40 μs) than •OH (E^0 = 1.8-2.7 V, half-life ~ 20 ns).[11] Additionally, persulfate-based AOP has higher radical formation yield, lower cost of transport and storage, and is less influenced by the reaction conditions such as pH, persulfate dosage, and background constitutes.[11] Considering the prominent advantages of persulfate and inspired by its use in environmental engineering, we postulate that the nanozyme-like colorimetric strategy based on persulfate activation could facilitate faster and more sensitive biomolecule detection. So far, persulfate has not been used in nanozyme-like colorimetric detections.

Glutathione (GSH) is an antioxidant that maintains the immune function in human cells, and its level in human serum is a widely used indicator in clinical diagnosis.[12-14] Using GSH as a representative biomolecule, we designed a nanozyme-like colorimetric sensing strategy based on peroxymonosulfate (PMS) activation on a Co-based metal-organic framework (MOF). Co-based MOF was chosen as the catalyst owing to the strong PMS activation efficiency of Co as well as the rich active sites and large surface areas of MOFs.[15,16]

We first synthesized the Co(BDC)$TED_{0.5}$ catalyst with porous prismatic morphology, featuring a large surface area and accessibility (Fig. S1 ESI†). The prismatic morphology of Co(BDC)$TED_{0.5}$ evolves with increasing hydrothermal reaction time (Fig. 1A). The Co(BDC)$TED_{0.5}$ with a 6-h reaction has a packed flat sheet structure (Fig. 1A (a)). After a 12-h reaction, Co(BDC)$TED_{0.5}$ nanosheets form curly edges (Fig. 1A (b)). As the reaction time extends to 24 h, the nanosheets become crumpled, forming a 3D porous architecture with loosely packed layers (Fig. 1A (c)). However, after a 48-h hydrothermal reaction, the nanosheets become less crumpled, close to the Co(BDC)$TED_{0.5}$ with a 6-h reaction time (Fig. 1A (d)). The

[a] State Key Laboratory of Pollution Control and Resource Reuse, School of the Environment, Nanjing University, Nanjing 210046, China
[b] Jiangsu Province Hospital on Integration of Chinese and West Medicine, Nanjing 210028, China
[c] Department of Civil and Environmental Engineering, Rice University, Houston, TX 77005, United States
[d] College of Urban and Environmental Sciences, Peking University, Beijing 100871, China
Electronic Supplementary Information (ESI) available. See DOI: 10.1039/x0xx00000x

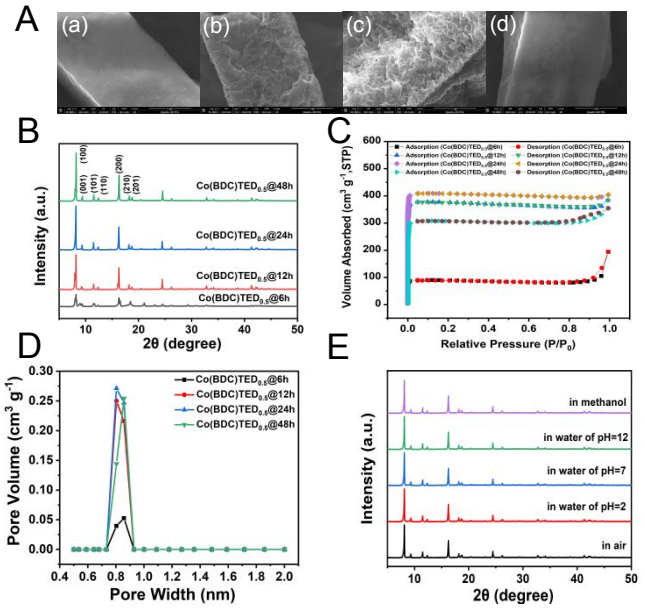

Fig. 1 (A) The FESEM images of (a) Co(BDC)TED$_{0.5}$@6h, (b) Co(BDC)TED$_{0.5}$@12h, (c) Co(BDC)TED$_{0.5}$@24h, and (d) Co(BDC)TED$_{0.5}$@48h. (B) PXRD profiles. (C) N_2 adsorption–desorption isotherms. (D) Pore size distribution of Co(BDC)TED$_{0.5}$ samples. (E) PXRD profiles of Co(BDC)TED$_{0.5}$@24h in different solutions.

formation of Co(BDC)TED$_{0.5}$ was supported by the characteristic PXRD peaks at 8.3°, 9.2°, 11.5°and 16.3° (Fig. 1B CCDC No. 661865).[17] The N_2 adsorption-desorption isotherms of Co(BDC)TED$_{0.5}$ are reversible type I isotherms, characteristic of microporous materials (Fig. 1C).[18] Among four Co(BDC)TED$_{0.5}$ samples with different hydrothermal reaction time, the Co(BDC)TED$_{0.5}$@24h has the highest specific surface area of 1084.54 $m^2\ g^{-1}$ (Fig. 1C) and total pore volumes of 0.63 $cm^3\ g^{-1}$ (Fig. 1D). This can be attributed to its crumpled sheet and the loosely stacked layer structure (Fig. 1A). The C, N, O, and Co elements are evenly distributed throughout the whole prism of Co(BDC)TED$_{0.5}$ (Fig. S2, ESI†). The structure of Co(BDC)TED$_{0.5}$@24h is stable in methanol and in water solution at pH of 2.0, 7.0, and 12.0 (Fig. 1E).

The catalytic activity of Co(BDC)TED$_{0.5}$ on PMS activation was examined using TMB as the colorimetric probe (Fig. 2A). The oxidation of colorless TMB mediated by PMS activation on Co(BDC)TED$_{0.5}$ leads to the formation of blue oxTMB with a characteristic absorbance at 652 nm (Fig. 2B). Co(BDC)TED$_{0.5}$@24h has the highest catalytic activity among all Co(BDC)TED$_{0.5}$ samples, which can be attributed to its highest specific surface area and pore volumes. This result also suggests that the reactions occur within the pores. The catalytic activity of Co(BDC)TED$_{0.5}$@24h was also compared with that of other Co-based materials, including $Co(NO_3)_2$, $CoFe_2O_4$, Co_3O_4, and $Co(OH)_2$ (Fig. S3, ESI†). Under the same reaction conditions, Co(BDC)TED$_{0.5}$@24h had the highest catalytic activity among these Co-based materials. In addition, there are no apparent changes in the PXRD and SEM-EDX profiles before and after

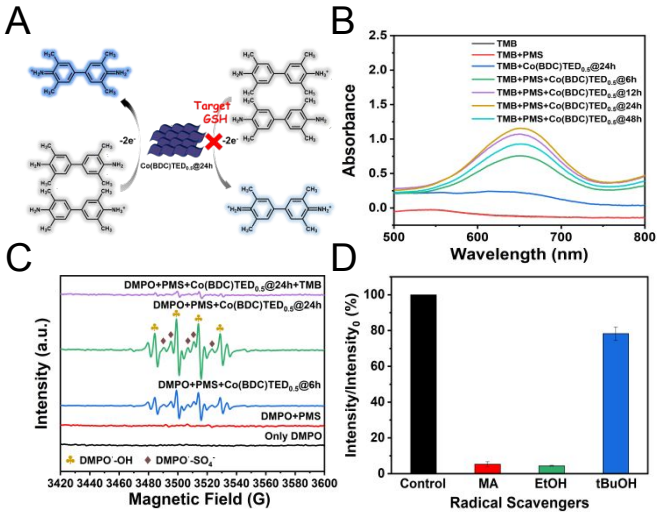

Fig. 2 (A) Schematic catalytic mechanism of Co(BDC)TED$_{0.5}$ as a catalyst. (B) UV−vis absorption spectra of different systems containing Co(BDC)TED$_{0.5}$. (C) EPR spectra of PMS activation on Co(BDC)TED$_{0.5}$ under different conditions with DMPO. (D) Inhibitory effect of radical scavengers on TMB oxidation by PMS activation on Co(BDC)TED$_{0.5}$@24h.

the catalytic reaction of Co(BDC)TED$_{0.5}$@24h (Fig. S2, S4 and S5, ESI †). Thus, Co(BDC)TED$_{0.5}$@24h was chosen to construct the colorimetric sensor for GSH detection in the following work.

PMS activation on Co(BDC)TED$_{0.5}$ induces the formation of •OH (a_N = 15.03 G and $a_{\beta\text{-}H}$ = 14.69 G) and $SO_4^{\bullet-}$ (a_N = 13.62 G,$a_{\beta\text{-}H}$ = 10.18 G, $a_{\gamma\text{-}H1}$ = 1.52 G, and $a_{\gamma\text{-}H2}$ = 0.81 G)[19, 20] (Fig. 2C), but little superoxide radical ($\bullet O_2^-$) as shown in the electron paramagnetic resonance (EPR) spectra (Fig. S6, ESI†). Co(BDC)TED$_{0.5}$@24h has stronger •OH and $SO_4^{\bullet-}$ signals than Co(BDC)TED$_{0.5}$@6h, consistent with its higher catalytic activity. The free radical quenching experiments show that $SO_4^{\bullet-}$ is the predominant radical in the oxidation of TMB mediated by PMS activation on Co(BDC)TED$_{0.5}$@24h (Fig. 2D). Density functional theory (DFT) results suggest three favorable pathways of PMS activation on Co(BDC)TED$_{0.5}$@24h (Fig. S7, ESI†). Pathway I mainly generates $SO_4^{\bullet-}$, which has the lowest energy requirement of 1.23 eV. Pathway II is the main pathway for •OH formation, and the energy requirement is 1.78 eV. $^1O_2$ generation by PMS activation (i.e., pathway III) is less favorable than $SO_4^{\bullet-}$ and •OH due to the high energy requirement of 2.31 eV. Thus, PMS activation on Co(BDC)TED$_{0.5}$@24h mainly generates $SO_4^{\bullet-}$ and •OH, consistent with the EPR data.

The steady-state kinetics of TMB oxidation mediated by PMS activation on Co(BDC)TED$_{0.5}$@24h was examined by independently altering the concentrations of the substrates (i.e., PMS and TMB) (Fig. S8 and S9, ESI†). At fixed PMS or TMB concentration, the steady-state kinetics of the reaction can be well fitted by the Michaelis-Menten equation ($R^2 > 0.99$), which is used to describe the steady-state kinetics of horseradish peroxidase (HRP) or nanozymes.[1, 21, 22] Thus, the oxidation of TMB by PMS activation on Co(BDC)TED$_{0.5}$@24h can be

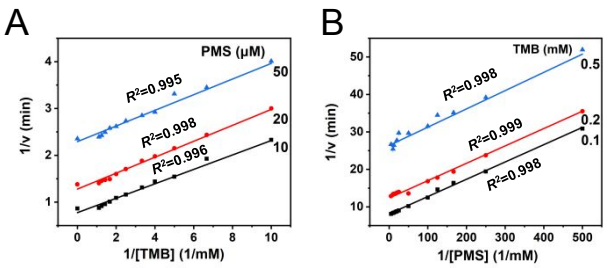

Fig. 3 Double-reciprocal plots for Co(BDC)TED$_{0.5}$@24h activity fitted at fixed concentrations of (A) PMS and (B) TMB.

considered as a bi-substrate nanozyme-like reaction. The parallel double-reciprocal plots of Co(BDC)TED$_{0.5}$@24h (Fig. 3) and the negligible Dalziel coefficient (*i.e.*, 0.00164) (Fig. S10, ESI†) suggest that the reaction is controlled by the ping-pong mechanism. [1, 22] The Michaelis–Menten constant (K_m) and maximum catalytic velocity (V_{max}) were then determined.[1] The K_m values are used to probe the affinity of substrates with enzymes. Substrates with higher affinity with enzymes have lower K_m values.[1] The K_m values of Co(BDC)TED$_{0.5}$@24h are 0.19 mM for TMB and 3.77×10^{-3} mM for PMS, respectively (Table 1). The K_m values of Co(BDC)TED$_{0.5}$@24h for TMB is slightly lower than HRP and common nanozymes (Table 1[1, 23-28]). The K_m values of Co(BDC)TED$_{0.5}$@24h for PMS are at least two orders of magnitude lower than the K_m values of HRP/nanozymes for H_2O_2. This result suggests that PMS has a much higher affinity to Co(BDC)TED$_{0.5}$@24h than H_2O_2 to HRP/nanozymes. The V_{max} value of TMB oxidation mediated by Co(BDC)TED$_{0.5}$@24h is 27.17×10^{-8} M s^{-1}, significantly higher than the HRP/nanozymes (Table 1). The catalytic efficiency of enzymes can be quantitatively evaluated using V_{max}/K_m. The V_{max}/K_m value of PMS activation on Co(BDC)TED$_{0.5}$@24h is 69.20×10^{-3} s^{-1}, which is 5,364 times higher than that of H_2O_2 activation on Co(BDC)TED$_{0.5}$@24h, 1.29×10^{-5} s^{-1}. It is also 3,460 times higher than the value for H_2O_2 activation by HRP (0.02×10^{-3} s^{-1}) and at least 202 times higher than previously reported values for H_2O_2 activation by nanozymes. This result suggests that Co(BDC)TED$_{0.5}$@24h has a strong affinity to TMB and PMS, especially PMS. The catalytic activation of PMS on Co(BDC)TED$_{0.5}$@24h is much more efficient than H_2O_2 activation by HRP/nanozymes.

Table 1 Comparison of kinetic parameters of PMS activation on Co(BDC)TED$_{0.5}$@24h with H_2O_2 activation on HRP and nanozymes.

Catalyst	Substrate	K_m (mM)	V_{max} (×10^{-8} M s^{-1})	V_{max}/K_m (×10^{-5} s^{-1})
Co(BDC)TED$_{0.5}$@24h	PMS	3.77×10^{-3}	26.09	6920.42
	TMB	0.19	30.02	158.00
Co(BDC)TED$_{0.5}$@24h	H_2O_2	3.14	4.05	1.29
	TMB	0.26	3.57	13.73
HRP[1]	H_2O_2	3.7	8.71	2.35
	TMB	0.434	10.00	23.04
Fe_3O_4[23]	H_2O_2	6.66	12.9	1.94
	TMB	0.295	0.72	2.44
Cys-MoS_2[24]	H_2O_2	1.98	1.52	0.77
	TMB	0.270	1.41	5.22
Fe-MIL-88NH_2[25]	H_2O_2	0.206	7.04	34.17
	TMB	0.284	10.47	36.87
$Pt_{0.1}$/Au NPs[26]	H_2O_2	0.436	0.0664	0.15
	TMB	0.44	16.51	37.52
Fe-N-C single atom[27]	H_2O_2	12.2	35.6	2.92
	TMB	3.6	116	32.22
Single-atom Pd/CeO_2[28]	H_2O_2	4.49	31.8	7.08
	TMB	0.227	38.1	167.84

We then designed a colorimetric sensor for GSH detection based on the highly efficient nanozyme-like reaction mediated by the activation of PMS on Co(BDC)TED$_{0.5}$@24h. The detection condition of the sensor was optimized as follows: 5 μg mL^{-1} Co(BDC)TED$_{0.5}$@24h, 500 μM TMB, 50 μM PMS, pH 5.0, and 8 min under room temperature (Fig. S11, ESI†). GSH effectively quenches $SO_4^{\bullet-}$ and •OH generated by PMS activation and reduces oxTMB to TMB by hydrogen donation[5, 8, 29], mitigating the color change. Consistently, the characteristic absorbance of oxTMB gradually decreased with increasing GSH concentrations (Fig. 4A). As expected, the blue color of the sensor became less intense with increasing GSH concentration (Fig. 4B). The concentration of GSH and the absorbance difference linearly correlated in the range of 0.1-2 μM and 2-30 μM with R^2 of 0.993 and 0.998, respectively (Fig. 4C). The LOD of the senor was 20.8 nM ($3S_B/k$) and the LOQ was 69.3 nM ($10S_B/k$). Compared with commercial colorimetric assay and nanozyme-based colorimetric method for GSH detection, our sensor has lower LOD, shorter detection time, and wider pH range (Table S1, ESI†). Eighteen common amino acids were tested by the sensing system to examine the selectivity. L-Cysteine (Cys) and L-Homocysteine (Hcy) with the sulfydryl group can also mitigate the color change of the sensor, but not as significantly as GSH (Fig. S12, ESI†). Considering the GSH concentration in serum samples (1-10 mM) is orders of magnitudes higher than Cys and Hcy (30-200 μM). Thus, the potential cooccurrence of Cys and Hcy is expected to have minor impacts on GSH detection in

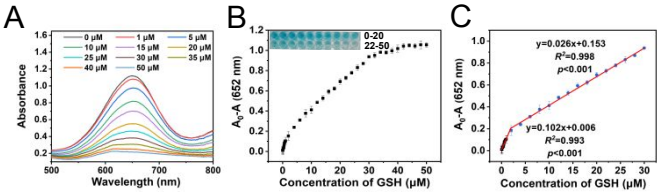

Fig. 4 (A) The UV absorption spectra of the colorimetric sensor with different concentrations of GSH (0-50 μM); (B) The absorbance difference of the sensor as a function of the GSH concentration, Inset: photographs of the sensor with different concentrations of GSH; (C) The linear correlations between the absorbance difference and the GSH concentration.

serum samples. The sensor performance remained stable at 97% after six runs (Fig. S13, ESI†).

This newly developed colorimetric sensor was applied for GSH detection in three human serum samples. The UV spectra and photos of the sensor after the addition of human serum as well as the analytical results are summarized in Table S2, ESI†. GSH concentrations in three diluted serum samples were measured to be 6.328 μM, 6.237 μM and 5.853 μM, respectively.

The spiked recoveries of the three serum samples are 92.0%—119.5% with relative standard deviation (RSD) ranging from 0.9 % to 6.0 %. The results demonstrate that the colorimetric sensor based on PMS activation on Co(BDC)TED$_{0.5}$@24h can be readily used in human serum samples for rapid, sensitive, and accurate GSH analysis. We further made paper strip sensors based on the same reaction to improve the convenience of GSH detection. The addition of 2 μL of GSH solution on the paper strip sensor leads to quick fading of the blue color in the detection zone (Fig. S14, ESI†). The color fading is generally proportional to the GSH concentration. The paper strip sensor can be potentially used for on-site detection of GSH.

In summary, we developed a nanozyme-like colorimetric sensing strategy based on persulfate activation for the first time. Compared to traditional H_2O_2-based nanozyme sensors, the high affinity between PMS and the catalyst as well as the high reactivity and long lifetime of $SO_4^{\bullet-}$ radical lead to the superior performance of PMS-based nanozyme-like sensor. By switching from H_2O_2 activation on nanozymes to catalytic persulfate activation, the colorimetric sensor provides significantly higher sensitivity, faster speed, and wider application ranges for detection. The resulting sensor was successfully applied for the detection of GSH in human serum samples both in solutions and on paper strips. The present strategy provides an excellent approach for GSH detection in biological samples and lays the foundation for applying persulfate in the sensitive screening and monitoring of biomolecules and biomarkers.

Zehui Deng: Investigation, Methodology, Writing- original draft; Qingling Xiao: Investigation; Heyun Fu: Methodology, Writing - review & editing; Shourong Zheng: Conceptualization, Writing- review & editing; Pedro J.J. Alvarez: Writing - review & editing, Funding acquisition; Dongqiang Zhu: W riting - review & editing; Zhaoyi Xu: Conceptualization, Methodology, Supervision, Funding acquisition, Writing - review & editing; Xiaolei Qu: Conceptualization, Methodology, Supervision, Funding acquisition, Writing - review & editing.

We are grateful to Professor Hui Wei from Nanjing University for the constructive comments and suggestions. This work was supported by the National Natural Science Foundation of China (Grant No. 42077164 and 21876075) and the NSF ERC, U.S.A on Nanotechnology-Enabled Water Treatment (EEC-1449500).

Conflicts of interest

There are no conflicts to declare.

Notes and references

1 L. Gao, J. Zhuang, L. Nie, J. Zhang, Y. Zhang, N. Gu, T. Wang, J. Feng, D. Yang, S. Perrett and X. Yan, Nat. Nanotechnol., 2007, 2, 577-583.
2 X. Niu, Y. He, X. Li, H. Zhao, J. Pan, F. Qiu and M. Lan, Sensor Actuat. B-Chem., 2019, 281, 445-452.
3 X. Xu, L. Wang, X. Zou, S. Wu, J. Pan, X. Li and X. Niu, Sensor Actuat. B-Chem., 2019, 298, 126876.
4 J. Li, L. Jiao, W. Xu, H. Yan, G. Chen, Y. Wu, L. Hu and W. Gu, Sensors and Actuators B: Chemical, 2021, 329, 129247.
5 N. Ye, S. Huang, H. Yang, T. Wu, L. Tong, F. Zhu, G. Chen and G. Ouyang, Anal. Chem., 2021, 93, 13981-13989.
6 H. Zou, T. Yang, J. Lan and C. Huang, Anal. Methods-UK, 2017, 9, 841-846.
7 Y. Ma, Z. Zhang, C. Ren, G. Liu and X. Chen, Analyst, 2012, 137, 485-489.
8 L. Wang, B. Li, Z. You, A. Wang, X. Chen, G. Song, L. Yang, D. Chen, X. Yu, J. Liu and C. Chen, Anal. Chem., 2021, 93, 11123-11132.
9 S. Singh, K. Mitra, A. Shukla, R. Singh, R. K. Gundampati, N. Misra, P. Maiti and B. Ray, Anal Chem, 2017, 89, 783-791.
10 J. Feng, P. Huang, S. Shi, K. Y. Deng and F. Y. Wu, Anal. Chim. Acta, 2017, 967, 64-69.
11 J. Lee, U. von Gunten and J. H. Kim, Environ. Sci. Technol., 2020, 54, 3064-3081.
12 Y. Liu, Y. Duan, A. D. Gill, L. Perez, Q. Jiang, R. J. Hooley and W. Zhong, Chem. Commun. (Camb), 2018, 54, 13147-13150
13 Y. Mei, H. Li, C. Z. Song, X. G. Chen and Q. H. Song, Chem. Commun. (Camb), 2021, 57, 10198-10201.
14 Y. Liu, Y. Duan, A. D. Gill, L. Perez, Q. Jiang, R. J. Hooley and W. Zhong, Chem. Commun. (Camb), 2018, 54, 13147-13150.
15 D. Yue, J. Zhu, D. Chen, W. Li, B. Qin, B. Zhang, D. Liu, X. Yang, Y. Zhang and Z. Wang, Dyes and Pigments, 2022, 206, 110655.
16 D. Yue, J. Zhu, D. Chen, W. Li, B. Qin, B. Zhang, D. Liu, X. Yang, Y. Zhang and Z. Wang, Dyes Pigments, 2022, 206, 110655.
17 S. Mutahir, C. Wang, J. Song, L. Wang, W. Lei, X. Jiao, M. A. Khan, B. Zhou, Q. Zhong and Q. Hao, Appl. Mater. Today, 2020, 21, 100813.
18 Z. Q. Bai, L.Y. Yuan, L. Zhu, Z. R. Liu, S. Q. Chu, L. R. Zheng, J. Zhang, Z. F. Chai and W. Q. Shi, J. Mater. Chem. A, 2015, 3, 525-534.
19 Z. Wei, F. A. Villamena and L. K. Weavers, Environ. Sci. Technol., 2017, 51, 3410-3417.
20 W. Qin, G. Fang, Y. Wang, T. Wu, C. Zhu and D. Zhou, Chemosphere, 2016, 148, 68-76.
21 H. Q. Zheng, C. Y. Liu, X. Y. Zeng, J. Chen, J. Lu, R. G. Lin, R. Cao, Z. J. Lin and J. W. Su, Inorg. Chem., 2018, 57, 9096-9104.
22 X. Liu, L. Huang, Y. Wang, J. Sun, T. Yue, W. Zhang and J. Wang, Sensor Actuat. B-Chem., 2020, 306, 127565.
23 Z. Zhang, X. Zhang, B. Liu and J. Liu, J. Am. Chem. Soc., 2017, 139, 5412-5419.
24 J. Yu, D. Ma, L. Mei, Q. Gao, W. Yin, X. Zhang, L. Yan, Z. Gu, X. Ma and Y. Zhao, J. Mater. Chem. B, 2018, 6, 487-498.
25 Y. L. Liu, X. J. Zhao, X. X. Yang and Y. F. Li, Analyst, 2013, 138, 4526-4531.
26 H. Chen, Q. Qiu, S. Sharif, S. Ying, Y. Wang and Y. Ying, ACS Appl. Mater. Inter., 2018, 10, 24108-24115.
27 Y. Chen, L. Jiao, H. Yan, W. Xu, Y. Wu, L. Zheng, W. Gu and C. Zhu, Anal. Chem., 2021, 93, 12353-12359.
28 H. Ruan, S. Zhang, H. Wang, J. Pei, R. Zhao, X. Mu, H. Wang and X. Zhang, ACS Appl. Nano Mater., 2022, 5, 6564-6574.
29 Y. Mei, H. Li, C. Z. Song, X. G. Chen and Q. H. Song, Chem. Commun. (Camb), 2021, 57, 10198-10201.